Single-shot interferometric approach to background free broadband coherent anti-Stokes Raman scattering spectroscopy*

Young Jong Lee and Marcus T. Cicerone

Polymers Division, National Institute of Standards and Technology, Gaithersburg, MD 20899
yjlee@nist.gov, cicerone@nist.gov

Abstract: We introduce a single-shot interferometric approach to suppress the nonresonant background (NRB) contribution to a broadband coherent anti-Stokes Raman scattering (CARS) spectrum; this single-shot approach is conducive to rapid imaging. A pulse shaper prepares a narrowband pulse with two spectral components of differing phase. When the CARS fields generated by these two out-of-phase components are optically mixed, NRB signal is greatly reduced while a resonant CARS signal remains with minimal attenuation. We discuss and demonstrate two model schemes for the interfering pulse components: (1) two pulses with different bandwidths and the same center frequency (*ps-fs* scheme) and (2) two pulses with the same bandwidth and shifted center frequencies (*ps-ps* scheme). In both schemes, only the resonant signal from the "3-color" CARS mechanism survives. The resonant signal from "2-color" CARS mechanism vanishes along with the NRB. We discuss optimization conditions for signal intensity and shape of resonant CARS peaks. Experimental CARS spectra of c-hexane and benzonitrile demonstrate feasibility of these approaches.

OCIS codes: (300.6230) Spectroscopy, coherent anti-Stokes Raman scattering; (320.5540) Pulse shaping.

References and links

1. A. Zumbusch, G. R. Holtom, and X. S. Xie, "Three-dimensional vibrational imaging by coherent anti-Stokes Raman scattering," Phys. Rev. Lett. **82,** 4142-4145 (1999).
2. C. L. Evans, E. O. Potma, M. Puoris'haag, D. Cote, C. P. Lin, and X. S. Xie, "Chemical imaging of tissue in vivo with video-rate coherent anti-Stokes Raman scattering microscopy," Proc. Natl. Acad. Sci. USA **102,** 16807-16812 (2005).
3. J. X. Cheng, A. Volkmer, L. D. Book, and X. S. Xie, "Multiplex coherent anti-stokes Raman scattering microspectroscopy and study of lipid vesicles," J. Phys. Chem. B **106,** 8493-8498 (2002).
4. T. W. Kee and M. T. Cicerone, "Simple approach to one-laser, broadband coherent anti-Stokes Raman scattering microscopy," Opt. Lett. **29,** 2701-2703 (2004).
5. G. I. Petrov and V. V. Yakovlev, "Enhancing red-shifted white-light continuum generation in optical fibers for applications in nonlinear Raman microscopy," Opt. Express **13,** 1299-1306 (2005).
6. H. A. Rinia, M. Bonn, and M. Muller, "Quantitative multiplex CARS spectroscopy in congested spectral regions," J. Phys. Chem. B **110,** 4472-4479 (2006).
7. Y. J. Lee, Y Liu, and M. T. Cicerone, "Characterization of 3-color CARS in a 2-pulse broadband CARS spectrum," Opt. Lett. **32,** 3370-3372 (2007).
8. F. Ganikhanov, C. L. Evans, B. G. Saar, and X. S. Xie, "High-sensitivity vibrational imaging with frequency modulation coherent anti-Stokes Raman scattering (FM CARS) microscopy," Opt. Lett. **31,** 1872-1874 (2006).
9. J. X. Cheng, A. Volkmer, L. D. Book, and X. S. Xie, "An epi-detected coherent anti-stokes raman scattering (E-CARS) microscope with high spectral resolution and high sensitivity," J. Phys. Chem. B **105,** 1277-1280 (2001).
10. J. X. Cheng, L. D. Book, and X. S. Xie, "Polarization coherent anti-Stokes Raman scattering microscopy," Opt. Lett. **26,** 1341-1343 (2001).
11. A. Volkmer, L. D. Book, and X. S. Xie, "Time-resolved coherent anti-Stokes Raman scattering microscopy: Imaging based on Raman free induction decay," Appl. Phys. Lett. **80,** 1505-1507 (2002).

#102753 - $15.00 USD Received 14 Oct 2008; revised 28 Nov 2008; accepted 4 Dec 2008; published 23 Dec 2008

12. C. L. Evans, E. O. Potma, and X. S. N. Xie, "Coherent anti-Stokes Raman scattering spectral interferometry: determination of the real and imaginary components of nonlinear susceptibility $\chi^{(3)}$ for vibrational microscopy," Opt. Lett. **29,** 2923-2925 (2004).
13. E. O. Potma, C. L. Evans, and X. S. Xie, "Heterodyne coherent anti-Stokes Raman scattering (CARS) imaging," Opt. Lett. **31,** 241-243 (2006).
14. D. Oron, N. Dudovich, and Y. Silberberg, "Femtosecond phase-and-polarization control for background-free coherent anti-Stokes Raman spectroscopy," Phys. Rev. Lett. **90,** 213902 (2003).
15. B. C. Chen and S. H. Lim, "Optimal laser pulse shaping for interferometric multiplex coherent anti-stokes Raman scattering microscopy," J. Phys. Chem. B **112,** 3653-3661 (2008).
16. T. W. Kee, H. X. Zhao, and M. T. Cicerone, "One-laser interferometric broadband coherent anti-Stokes Raman scattering," Opt. Express **14,** 3631-3640 (2006).
17. J. P. Ogilvie, E. Beaurepaire, A. Alexandrou, and M. Joffre, "Fourier-transform coherent anti-Stokes Raman scattering microscopy," Opt. Lett. **31,** 480-482 (2006).
18. H. Kano and H. Hamaguchi, "Dispersion-compensated supercontinuum generation for ultrabroadband multiplex coherent anti-Stokes Raman scattering spectroscopy," J. Raman Spectrosc. **37,** 411-415 (2006).
19. G. L. Eesley, *Coherent Raman Spectroscopy* (Pergamon Press, Oxford 1981).
20. D. Oron, N. Dudovich, D. Yelin, and Y. Silberberg, "Narrow-band coherent anti-stokes Raman signals from broad-band pulses," Phys. Rev. Lett. **88,** 063004 (2002).
21. A. Morresi, L. Mariani, M. R. Distefano, and M. G. Giorgini, "Vibrational-Relaxation Processes in Isotropic Molecular Liquids - A Critical Comparison," J. Raman Spectrosc. **26,** 179-216 (1995).
22. J. M. Dudley, G. Genty, and S. Coen, "Supercontinuum generation in photonic crystal fiber," Rev. Mod. Phys. **78,** 1135-1184 (2006).
23. Y. J. Lee and M. T. Cicerone, "Vibrational dephasing time imaging by time-resolved broadband coherent anti-Stokes Raman scattering microscopy," Appl. Phys. Lett. **92,** 041108 (2008).
24. Certain equipment is identified in this Letter to specify adequately the experimental details. Such identification does not imply recommendation by the National Institute of Standards and Technology, nor does it imply that the equipment is necessarily the best available for this purpose.
25. B. von Vacano, L. Meyer, and M. Motzkus, "Rapid polymer blend imaging with quantitative broadband multiplex CARS microscopy," J. Raman Spectrosc. **38,** 916-926 (2007).
26. M. Jurna, J. P. Korterik, C. Otto, and H. L. Offerhaus, "Shot noise limited heterodyne detection of CARS signals," Opt. Express **15,** 15207-15213 (2007).

1. Introduction

Coherent anti-Stokes Raman scattering (CARS) microscopy has been used widely for noninvasive, label-free, three-dimensional chemical imaging of biological and polymeric samples [1]. CARS microscopy is based on third-order nonlinear vibrational spectroscopy, where the signal is enhanced when difference between pump and Stokes frequencies is close to a molecular vibrational frequency. Single frequency CARS approaches use two picosecond pulses tuned to a specific Raman mode to achieve fast data acquisition speed and high sensitivity [2]. However, both quantitative and qualitative Raman spectrum analysis of complex media including biological samples generally requires spectral data over a wide frequency range at a single measurement. Multiplex and broadband CARS approaches have been demonstrated to provide a broad Raman spectrum at a single measurement by overlapping a narrowband picosecond pulse and a broadband pulse [3-6]. The multiplex measurement techniques show great advantages for analysis of crowded Raman spectra in the fingerprint region (500 - 1800 cm^{-1}) [6].

For both single-frequency and broadband CARS approaches, the resonantly enhanced signal of interest is accompanied by a nonresonant background (NRB) signal, which is due to an instantaneous coherent electronic response of the sample. The NRB poses a significant interference to the resonant Raman signal and often overwhelms weak resonant signals, leading to significant reduction in imaging contrast and sensitivity. The NRB in a broadband CARS spectrum is particularly difficult to characterize because the CARS spectrum is directly affected by the continuum pulse, whose intensity and phase is often unstable and may contain multiple modes [7]. Several experimental approaches have been established for reducing the NRB contribution, including frequency-modulation [8], epi-detection [9], polarization control [10], time-resolved [11], and interference [12] CARS techniques. Of these, all but the frequency-modulation technique is available to broadband CARS, but each of these approaches has drawbacks. Epi-detection suppresses the contribution of bulk solvent but

#102753 - $15.00 USD Received 14 Oct 2008; revised 28 Nov 2008; accepted 4 Dec 2008; published 23 Dec 2008

yields signal only from features small compared to the wavelength of the scattering light. Polarization control and time-resolved CARS techniques can attenuate resonant signal significantly.

Interferometric CARS offers the possibility of detecting NRB-free CARS signal with minimal attenuation of resonant signal intensity. Conventional interferometric detection methods combine the signal of a CARS field from the sample of interest and a well-controlled reference field. Heterodyne methods use a strong reference field (local oscillator) to enhance the resonant signal in addition to separating out the phase information [13]. However, when a reference field is generated in a different medium, it is generally very difficult to account for differential phase shift and differential chirp over a broad frequency range, and to remove phase jitter. Generating signal and reference fields in the same sample obviates these problems. Silberberg et al. [14] have demonstrated and Lim et al. [15] have improved single pulse CARS techniques where NRB is reduced by interfering adjacent narrow spectral components of a single ultrashort laser pulse using a pulse shaper. In the single pulse technique, however, a spatial light modulator controls the whole frequency range of pump, Stokes, and probe, and therefore, the number of elements in the spatial light modulator limits the product of spectral resolution and spectral range. Cicerone et al. [16] have demonstrated a different approach to scanning interferometric broadband CARS microscopy by mixing signal and reference fields that are generated by a spectrally narrow pulse and a broad pulse for pump light, respectively, but this approach required phase scanning of one of the pump pulses to extract Fourier amplitudes of the signals generated. Recently, Ogilvie et al. [17] also demonstrated an interferometric Fourier transform method that was used in an imaging mode. The necessity of scanning the relative phase between two pulses in these types of methods typically increases the data acquisition time compared to a single spectral acquisition at each imaging point.

In this paper we describe single-shot interferometric approaches to suppress NRB contribution to a broadband CARS spectrum that does not require scanning the relative pulse phase and results in very little attenuation of resonance signal intensity. In these approaches, two probe pulse components are separately controlled by a pulse shaper and the CARS fields they generate are interferometrically mixed. We discuss characteristics of the interference CARS spectra depending on CARS mechanisms occurring in broadband CARS. We present two model schemes and discuss the optimization conditions for high resonant signal intensity of NRB-free broadband CARS spectra.

2. Theory

The CARS signal is induced by the third-order nonlinear polarization, $\mathbf{P}^{(3)}$, which is expressed as

$$\mathbf{P}^{(3)}(\omega_{aS}) = \int_{-\infty}^{\infty}\int_{-\infty}^{\infty}\int_{-\infty}^{\infty}\chi^{(3)}(\omega_p,\omega_S,\omega_{pr};\omega_{aS})\mathbf{E}(\omega_p)\mathbf{E}^{*}(\omega_S)\mathbf{E}(\omega_{pr}) \times\delta(\omega_p-\omega_S+\omega_{pr}-\omega_{aS})d\omega_p d\omega_S d\omega_{pr} \tag{1}$$

where $\chi^{(3)}$ is the third-order nonlinear susceptibility, $\mathbf{E}(\omega)$ are the electric field vectors, and the subscripts *p*, *S*, *pr*, and *aS* indicate pump, Stokes, probe, and anti-Stokes transitions, respectively. Recent studies [7,18] show that a broadband CARS signal can be generated by two different generation mechanisms as described in Fig. 1: (i) "2-color" CARS, where the pump and probe are provided by a narrowband pulse, and the continuum pulse constitutes the Stokes light; and (ii) "3-color" CARS, where pump and Stokes are provided by two different frequency components in the continuum pulse and the narrowband pulse serves as probe. Depending on the generation mechanism, the nonlinear polarization for CARS emission is expressed as follows:

$$P^{(3)}_{2-\text{color}}(\omega_{aS}) = \int_{-\infty}^{\infty}\int_{-\infty}^{\infty}\chi^{(3)}E_{\text{n}}(\omega_p)E_{\text{c}}^{*}(\omega_p+\omega_{pr}-\omega_{aS})E_{\text{n}}(\omega_{pr})\,d\omega_p d\omega_{pr} \tag{2}$$

#102753 - $15.00 USD Received 14 Oct 2008; revised 28 Nov 2008; accepted 4 Dec 2008; published 23 Dec 2008

$$P^{(3)}_{3\text{–color}}(\omega_{aS}) = \int_{-\infty}^{\infty}\int_{-\infty}^{\infty} \chi^{(3)} E_c(\omega_p) E_c^*(\omega_p + \omega_{pr} - \omega_{aS}) E_n(\omega_{pr})\, d\omega_p\, d\omega_{pr} \tag{3}$$

where $E_n(\omega)$ and $E_c(\omega)$ are the electric fields of the narrowband and continuum pulses. The nonlinear polarizations and electric fields are treated as scalar values for simplicity. The third-order nonlinear susceptibility, $\chi^{(3)}$, can be described as a function of (ω_p - ω_S) and can be expressed using parameters from a spontaneous Raman spectrum [19] as follows

$$\chi^{(3)}(\omega_p, \omega_S) = \chi^{(3)}_{NR} + \chi^{(3)}_R(\omega_p, \omega_S) = \chi^{(3)}_{NR} + \sum_i \frac{A_i}{[(\omega_p - \omega_S) - \Omega_{R,i}] + i\Gamma_i} \tag{4}$$

where $\chi^{(3)}_{NR}$ and $\chi^{(3)}_R$ are the nonresonant and resonant contributions, respectively, $\Omega_{R,i}$ is the frequency of the ith Raman mode, A_i is a constant representing the spontaneous Raman cross section, and Γ_i is the Raman linewidth. From energy conservation considerations, (ω_p - ω_S) = (ω_{aS} - ω_{pr}), and Eq. (4) can be expressed as a function of (ω_{aS} - ω_{pr}) as follows:

$$\chi^{(3)}(\omega_{aS}, \omega_{pr}) = \chi^{(3)}_{NR} + \sum_i \frac{A_i}{[(\omega_{aS} - \omega_{pr}) - \Omega_{R,i}] + i\Gamma_i} \tag{4'}$$

In broadband CARS spectroscopy, the spectral bandwidth of $E_c(\omega)$ is generally much larger than that of $E_n(\omega)$. Thus, the amplitude and the phase of $E_c^*(\omega_p + \omega_{pr} - \omega_{aS})$ is essentially constant within the integral over $d\omega_{pr}$ in Eqs. (2) and (3), when $E_c(\omega)$ is transform-limited and its spectral shape is smooth. Under these conditions the coupled double integrals in Eqs. (2) and (3) can be reasonably approximated as products of separate integrals. We make this assumption in the following (deviations from this approximation will be pointed out in the discussion of the *ps-fs* scheme below).

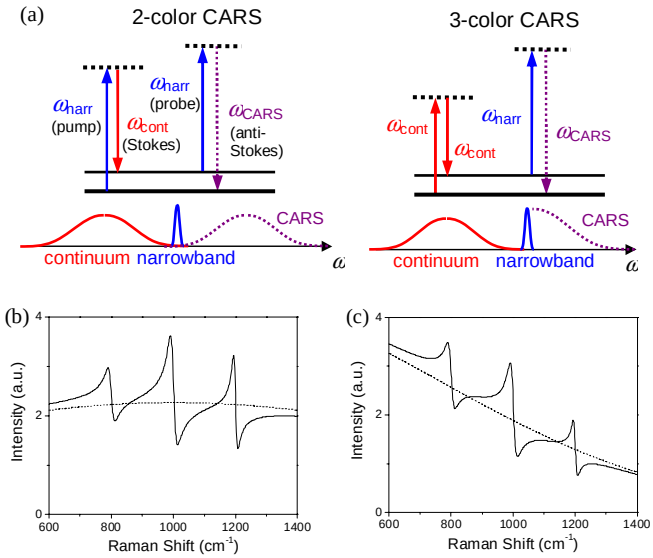

Fig. 1. (a) Schematic diagrams of 2- and 3-color CARS generation mechanisms in two-pulse broadband CARS spectroscopy. ω_{narr} and ω_{cont} represent photons from narrowband and continuum pulses respectively. CARS spectra are simulated via (b) 2-color and (c) 3-color mechanisms. The dashed lines indicate NRB contribution. See the text for the simulation parameters.

$$P^{(3)}_{2\text{–color}}(\omega_{aS}) = \int_{-\infty}^{\infty} E_n(\omega_p) E_c^*(\omega_p + \omega_{pr} - \omega_{aS})\, d\omega_p \int_{-\infty}^{\infty} \chi^{(3)}(\omega_{aS}, \omega_{pr}) E_n(\omega_{pr})\, d\omega_{pr} \tag{5}$$

#102753 - $15.00 USD Received 14 Oct 2008; revised 28 Nov 2008; accepted 4 Dec 2008; published 23 Dec 2008

$$P^{(3)}_{3\text{-color}}(\omega_{aS}) = \int_{-\infty}^{\infty} E_c(\omega_p) E_c^*(\omega_p + \omega_{pr} - \omega_{aS}) d\omega_p \int_{-\infty}^{\infty} \chi^{(3)}(\omega_{aS}, \omega_{pr}) E_n(\omega_{pr}) d\omega_{pr} \quad (6)$$

The 3-color and 2-color CARS signals differ in several ways; one is that the former always displays amplitude that decreases with increasing Raman shift due to the frequency-domain autocorrelation of the continuum pulse, expressed in the first integral of Eq. (6). Another difference, crucial in the context of this paper, is that the 2-color signal is generated with two photons from the narrow-band pulse, whereas 3-color uses only one. As we will see, this difference results in vanishing of all 2-color signal but survival of resonant 3-color signal under the condition required for NRB suppression.

Below we demonstrate two model cases in which we modify a "narrowband" pulse $E_n(\omega)$ into a superposition of two pulse components whose amplitudes and phases are independently controlled. In case (1) "*ps-fs*", two narrowband Gaussian pulses have different bandwidths and are located at the same center frequency. In case (2) "*ps-ps*", two narrowband Gaussian pulses have the same bandwidths and the center frequencies are separated from each other. In both model cases, the resulting CARS spectra show a strong interferometric behavior with the relative phase between the two pulse components. Below we describe the "*ps-fs*" and "*ps-ps*" cases using both analytical expressions and simulations of spectra. In the spectral simulations we use a Raman spectrum with three peaks centered at $\Omega_{R,1}$ = 800 cm^{-1}, $\Omega_{R,2}$ = 1000 cm^{-1}and $\Omega_{R,3}$ = 1200 cm^{-1}, with amplitudes $A_1 = A_3 = 0.5$, and $A_2 = 1$, and widths $\Gamma_1 = \Gamma_2$ = 10 cm^{-1} and Γ_3 = 5 cm^{-1}, we also assume $\chi^{(3)}_{NR}$ = 0.2. In all simulations the full-width-half-maximum (FWHM) of the narrowband pulse is set to be 5 cm^{-1} and the FWHM of the continuum pulse is set to be 2500 cm^{-1}. Both the narrowband and continuum pulses are assumed to be transform-limited Gaussian functions. Figure 1 shows simulated 2- and 3-color CARS spectra generated with a single narrowband *ps* probe pulse. This is given as reference for introduction to interferometric approaches using pairs of probe pulses.

2.1 ps-fs interference scheme

In the *ps-fs* scheme, $E_n(\omega)$ consists of two Gaussian pulses $E_{ps}(\omega)$ and $E_{fs}(\omega)$, where the bandwidths are significantly different but center frequencies are the same. The electric fields of the two Gaussian pulses are expressed as $E_{ps}(\omega) = E^0_{ps} \exp[-(2\ln 2)\times(\omega-\omega_c)^2/\Delta\omega^2_{ps}]$ and $E_{fs}(\omega) = E^0_{fs} \exp[-(2\ln 2)\times(\omega-\omega_c)^2/\Delta\omega^2_{fs}]$, where E^0_{ps} and E^0_{fs} are the peak field amplitudes, ω_c is the center frequency, and $\Delta\omega_{ps}$ and $\Delta\omega_{fs}$ are the FWHM of the intensity spectra. The overall electric field of the narrowband pulse can be written as

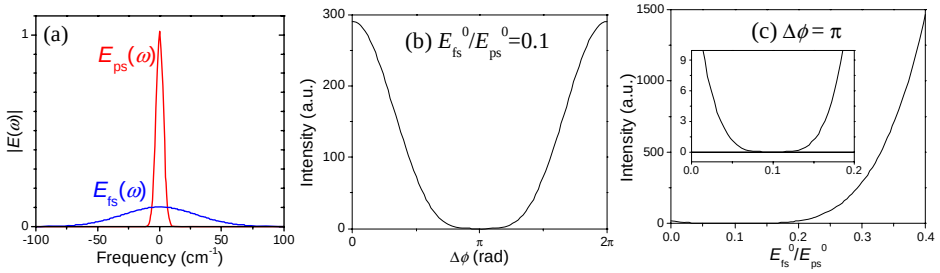

Fig. 2. (a) The electric fields $E_{ps}(\omega)$ and $E_{fs}(\omega)$ used in the *ps-fs* scheme, where $\Delta\omega_{ps}$ = 5 cm^{-1} and $\Delta\omega_{fs}$ = 50 cm^{-1}, respectively. NRB intensity is calculated as a function of (b) $\Delta\phi$ and (c) E^0_{fs}/E^0_{ps}. The inset of Fig. 2(c) shows the symmetry in NRB amplitude around the region of $E^0_{fs}/E^0_{ps} = 0.1\cdot$

$$E_n(\omega) = E_{ps}(\omega)e^{i\Delta\phi} + E_{fs}(\omega) \quad (7)$$

#102753 - $15.00 USD Received 14 Oct 2008; revised 28 Nov 2008; accepted 4 Dec 2008; published 23 Dec 2008

where $\Delta\phi$ is the phase difference between the two pulses. (Note that the *fs* pulse is considered as a component of the *narrowband* pulse.) We obtain expressions for 2-color or 3-color CARS emission intensity, $I(\omega_{aS}) \propto \left|P^{(3)}(\omega_{aS})\right|^2$, by combining Eq. (7) with Eqs. (5) or (6), respectively:

$$I_{\text{ps-fs}}^{2-\text{color}}(\omega_{aS},\Delta\phi) \propto \left|\int_{-\infty}^{\infty}\left[E_{\text{ps}}(\omega_p)\text{e}^{\text{i}\Delta\phi}+E_{\text{fs}}(\omega_p)\right]E_c^*(\omega_p+\omega_{pr}-\omega_{aS})d\omega_p \times\int_{-\infty}^{\infty}\chi^{(3)}(\omega_{aS},\omega_{pr})\left[E_{\text{ps}}(\omega_{pr})\text{e}^{\text{i}\Delta\phi}+E_{\text{fs}}(\omega_{pr})\right]d\omega_{pr}\right|^2 \tag{8}$$

$$I_{\text{ps-fs}}^{3-\text{color}}(\omega_{aS},\Delta\phi) \propto \left|\int_{-\infty}^{\infty}E_{\text{c}}(\omega_p)E_{\text{c}}^{\ *}(\omega_p+\omega_{pr}-\omega_{aS})d\omega_p \times\int_{-\infty}^{\infty}\chi^{(3)}(\omega_{aS},\omega_{pr})\left[E_{\text{ps}}(\omega_{pr})\text{e}^{\text{i}\Delta\phi}+E_{\text{fs}}(\omega_{pr})\right]d\omega_{pr}\right|^2 \tag{9}$$

The NRB contribution to the signal is obtained by replacing $\chi^{(3)}$ with $\chi_{NR}^{(3)}$ (a frequency-independent constant) in Eqs. (8) and (9). In 2-color and 3-color CARS, interference between the signals generated from $E_{\text{ps}}(\omega)$ and $E_{\text{fs}}(\omega)$ results in strong dependence of NRB intensity on both $\Delta\phi$ and $E_{\text{fs}}^0/E_{\text{ps}}^0$ as displayed in Fig. 2.

Figure 2(a) shows an example $E_{\text{n}}(\omega)$ composed of $E_{\text{ps}}(\omega)$ and $E_{\text{fs}}(\omega)$ with $\Delta\omega_{\text{ps}}$ = 5 cm^{-1}, $\Delta\omega_{\text{fs}}$ = 50 cm^{-1} and $E_{\text{fs}}^0/E_{\text{ps}}^0$ = 0.1 Figures 2(b) and 2(c) show NRB intensity as a function of $\Delta\phi$ and $E_{\text{fs}}^0/E_{\text{ps}}^0$ respectively. For any given value of $E_{\text{fs}}^0/E_{\text{ps}}^0$, the NRB contribution is minimized any time $\Delta\phi = \pi$, when the two pulses are out of phase. It is maximally suppressed only when $\Delta\phi = \pi$ and $\int_{-\infty}^{\infty}E_{\text{ps}}(\omega)\,d\omega = \int_{-\infty}^{\infty}E_{\text{fs}}(\omega)\,d\omega$. In the case shown in Fig. 2, $\Delta\omega_{\text{fs}}/\Delta\omega_{\text{ps}} = 10$, so the NRB signal vanishes at $E_{\text{fs}}^0/E_{\text{ps}}^0 = 0.1$. Inspection of Eq. (8) immediately shows that both resonant and nonresonant signals arising from the 2-color mechanism are eliminated under the conditions of NRB suppression since the first integral term in Eq. (8) becomes zero under these conditions independent of the value of $\chi^{(3)}(\omega_{aS}, \omega_{pr})$. For 3-color CARS signal, described by Eq. (9), the integral involving $E_{\text{ps}}(\omega)$ and $E_{\text{fs}}(\omega)$ can have a non-zero value under the conditions of NRB suppression due to the presence of the term $\chi^{(3)}(\omega_{aS}, \omega_{pr})$.

As discussed above, the NRB contributions generated using a pulse pair such as $E_{\text{fs}}(\omega)$ and $E_{\text{ps}}(\omega)$ depicted in Fig. 2(a), will be of equal amplitude and will cancel because the two contributions are phase shifted by π with respect to each other. In such a spectrum, the 3-color resonant Raman features generated by $E_{\text{fs}}(\omega)$ are smeared out, yielding a more-or-less spectrally flat signal, while the resonant Raman features generated by $E_{\text{ps}}(\omega)$ are sharp and dispersive, characteristic of high-resolution CARS spectra. As with the NRB, the resonant components are π out of phase, but the resonant signal from $E_{\text{fs}}(\omega)$ only slightly attenuates the resonant signal from $E_{\text{ps}}(\omega)$ due to the flat line shape of the $E_{\text{fs}}(\omega)$-derived signal, and the fact that the latter is spread out over a wider frequency range. Thus, the surviving signal is composed primarily of contributions from the resonant CARS signal due to the *ps* pulse.

#102753 - $15.00 USD Received 14 Oct 2008; revised 28 Nov 2008; accepted 4 Dec 2008; published 23 Dec 2008

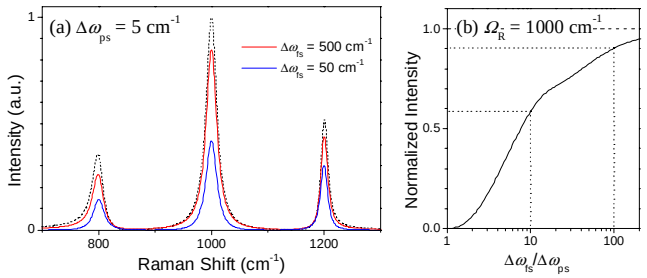

Fig. 3. (a) NRB suppressed 3-color CARS spectra in the *ps-fs* scheme for two $\Delta\omega_{fs}$ values of 50 cm^{-1} (blue) and 500 cm^{-1} (red) when $\Delta\omega_{ps}$ = 5 cm^{-1}. The dotted line is the 3-color CARS spectrum calculated only with resonant signal [$\chi_{NR}^{(3)}$ = 0] generated with a single *ps* pulse. (b) Semi-log plot of calculated peak intensity of the Raman mode at 1000 cm^{-1} as a function of $\Delta\omega_{fs}$ while $\Delta\phi = \pi$ and $E_{fs}^0 / E_{ps}^0 = \Delta\omega_{ps}/\Delta\omega_{fs}$.

Figure 3(a) shows 3-color CARS spectra calculated using this NRB elimination scheme, with $\Delta\omega_{ps}$ = 5 cm^{-1}, and with $\Delta\omega_{fs}$ = 50 cm^{-1} or 500 cm^{-1}. The peak shapes are not significantly impacted by the relative widths the *ps* and *fs* probe components, but the larger value of $\Delta\omega_{fs}$ yields an increased recovery of resonant Raman signal. This increased recovery with broad *fs* probe pulse can be seen more clearly in Fig. 3(b), where the peak intensity of the Raman mode at 1000 cm^{-1} is plotted as a function of increasing $\Delta\omega_{fs}/\Delta\omega_{ps}$, $\Delta\omega_{ps}$ being fixed at 5 cm^{-1}. The peak intensity asymptotically increases towards 100% recovery of the pure resonant signal, which is shown as the dotted line in Fig. 3(a). The dotted line, as a reference, is calculated with $\chi_{NR}^{(3)}$ = 0 and $E_n(\omega)$ composed only of $E_{ps}(\omega)$, with $E_{ps}(\omega)$ having an integrated intensity equal to that of $E_{ps}(\omega)$+$E_{fs}(\omega)$ in the corresponding solid line. Figure 3 shows that with $\Delta\omega_{fs}$ = 50 cm^{-1} and 500 cm^{-1}, the peak intensity of the Raman mode at 1000 cm^{-1} reach 59% and 90% intensities of the pure resonant CARS amplitude, respectively. However, we note that it may not be possible to completely suppress the NRB for a large $\Delta\omega_{fs}$ (e.g. $\Delta\omega_{fs}$ = 500 cm^{-1}). In cases where there is non-negligible variation in amplitude and phase of the continuum pulse within frequency intervals equal to the broad *fs* pulse bandwidth, the two integrals in Eqs. (5) and (6) cannot be separated to good approximation, and the simplified analysis presented here does not necessarily hold. However, depending on the details of the shape of the continuum pulse, we may still expect a significant decrease in NRB contribution for much of the CARS signal bandwidth by adjusting the relative intensity and phase of the two narrowband pulse components.

2.2 ps-ps *interference scheme*

In the *ps-ps* scheme, $E_n(\omega)$ consists of two narrowband Gaussian pulses whose bandwidths are the same but whose center frequencies are shifted, as shown in Fig. 4(a). The electric fields of the *ps* pulses can be expressed as $E_{ps1}(\omega) = E_{ps}^0 \exp[-(2\ln 2)\times(\omega - \omega_c + \Delta\omega_c/2)^2 / \Delta\omega_{ps}^2]$ and $E_{ps2}(\omega) = E_{ps}^0 \exp[-(2\ln 2)\times(\omega - \omega_c - \Delta\omega_c/2)^2 / \Delta\omega_{ps}^2]$, where $\Delta\omega_c$ is the frequency separation between the two pulses. The overall electric field of the narrowband pulse is thus written as:

$$E_n(\omega) = E_{ps1}(\omega)e^{i\Delta\phi} + E_{ps2}(\omega) \tag{10}$$

We obtain expressions for the 2-color or 3-color CARS signal intensity in the *ps-ps* scheme when we combine Eq. (10) with Eqs. (5) or (6), respectively:

#102753 - $15.00 USD Received 14 Oct 2008; revised 28 Nov 2008; accepted 4 Dec 2008; published 23 Dec 2008

$$I_{\text{ps-ps}}^{2-\text{color}}(\omega_{aS},\Delta\phi) \propto \left| \int_{-\infty}^{\infty} \left[E_{\text{ps1}}(\omega_p) \mathrm{e}^{\mathrm{i}\Delta\phi} + E_{\text{ps2}}(\omega_p) \right] E_{\text{c}}^{\,*}(\omega_p + \omega_{pr} - \omega_{aS}) d\omega_p \right.$$
$$\left. \times \int_{-\infty}^{\infty} \chi^{(3)}(\omega_{aS},\omega_{pr}) \left[E_{\text{ps1}}(\omega_{pr}) \mathrm{e}^{\mathrm{i}\Delta\phi} + E_{\text{ps2}}(\omega_{pr}) \right] d\omega_{pr} \right|^2 \tag{11}$$

$$I_{\text{ps-ps}}^{3-\text{color}}(\omega_{aS},\Delta\phi) \propto \left| \int_{-\infty}^{\infty} E_{\text{c}}(\omega_p) E_{\text{c}}(\omega_p + \omega_{pr} - \omega_{aS})^{*} d\omega_p \right.$$
$$\left. \times \int_{-\infty}^{\infty} \chi^{(3)}(\omega_{aS},\omega_{pr}) \left[E_{\text{ps1}}(\omega_{pr}) \mathrm{e}^{\mathrm{i}\Delta\phi} + E_{\text{ps2}}(\omega_{pr}) \right] d\omega_{pr} \right|^2 \tag{12}$$

When the NRB suppression condition, $\int_{-\infty}^{\infty} \left[E_{\text{ps1}}(\omega_p) \mathrm{e}^{\mathrm{i}\Delta\phi} + E_{\text{ps2}}(\omega_p) \right] d\omega_p = 0$, is satisfied, the entire resonant 2-color CARS spectrum, as well as NRB contributions from both 2-color and 3-color mechanisms vanish, as with the *ps-fs* scheme. In the *ps-ps* scheme, the NRB suppression condition is fulfilled when $\Delta\phi = \pi$ and $|E_{\text{ps1}}| = |E_{\text{ps2}}|$ irrespective of the value of $\Delta\omega_{\text{c}}$, provided the amplitude of the NRB does not change significantly over the interval $\Delta\omega_{\text{c}}$.

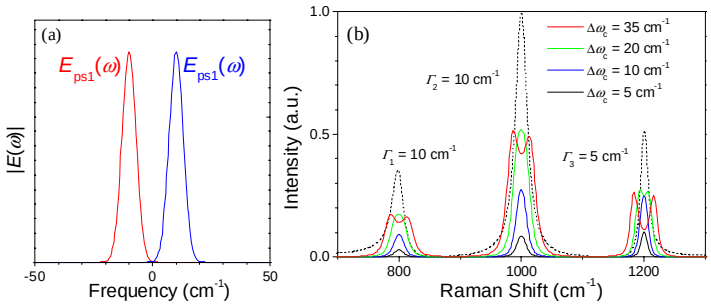

Fig. 4. (a) Electric field amplitudes $E_{\text{ps1}}(\omega)$ and $E_{\text{ps2}}(\omega)$ used in the *ps-ps* scheme, where $\Delta\omega_{\text{ps}}$ = 5 cm^{-1}. (b) Simulated 3-color CARS spectra for various $\Delta\omega_{\text{c}}$. As a reference (the dotted line), a 3-color CARS spectrum is calculated for $\chi_{NR}^{(3)} = 0$ by a single *ps* pulse for $E_{\text{n}}(\omega)$ when the pulse energy is assumed to be equal to the sum of those of $E_{\text{ps1}}(\omega)$ and $E_{\text{ps2}}(\omega)$ for the other *ps-ps* simulations.

Figure 4 shows 3-color CARS spectra calculated for $\Delta\phi = \pi$ and various values of $\Delta\omega_{\text{c}}$. This NRB suppression condition for the *ps-ps* scheme is similar in nature to the pulse shaping approach demonstrated by Silberberg et al. [20], where the phase of a Gaussian-like probe beam was altered by π at the center frequency of the pulse. Despite slight differences in pulse shape and phase function, the π step phase across adjacent spectral components (see also Refs. [14,15]) yields a probe pulse that is very similar to the pulse generated in the *ps-ps* scheme discussed here, with $\Delta\omega_{\text{c}} = \Delta\omega_{\text{ps}}$, and can thus be considered a special case of that scheme. (See below.) Here we show that as $\Delta\omega_{\text{c}}$ is increased, the signal intensity increases. However, when the spacing exceeds twice the FWHM of the non-interferometric spectral feature, i.e. $\Delta\omega_{\text{c}} > 2[\Gamma^{-2} + (\Delta\omega_{\text{ps}})^2)]^{1/2}$, there is no further increase in signal amplitude, and a peak splitting artifact emerges, as clearly demonstrated by the Raman mode at 1200 cm^{-1}. The maximum peak intensity in the *ps-ps* scheme is close to 100% of the pure resonant [$\chi_{NR}^{(3)} = 0$] CARS intensity calculated with one of two separate *ps* pulses. If, for consistency with the *ps-fs* scheme discussion, we compare calculated signal recovery against signal calculated with a single *ps* pulse having the same pulse energy as the sum of the geminate $E_{\text{n}}(\omega)$ pulses, we calculate a maximum signal recovery of 50%. The signal increase and peak splitting with increased $\Delta\omega_{\text{c}}$ in the *ps-ps* 3-color CARS can be understood as a result of interactions between two out-of-phase resonant CARS polarizations. When $\Delta\omega_{\text{c}}$ is large and the two peaks are

#102753 - $15.00 USD Received 14 Oct 2008; revised 28 Nov 2008; accepted 4 Dec 2008; published 23 Dec 2008

sufficiently separated, both peaks appear individually and the peak heights remain unaffected. For a small $\Delta\omega_c$, destructive interference in the overlap region of the two pulse spectra can reduce the total (time-averaged) light intensity. However, this destructive interference leads to a signal reduction of only a factor of two between $\Delta\omega_c$ = 5 cm^{-1} and 20 cm^{-1}, while the CARS peak height ratio for the peaks resulting from these conditions is six. This additional increase is a result of a faster-rising electric field in the time domain for $\Delta\omega_c$ = 20 cm $^{-1}$, and thus a more efficient sampling of the resonant Raman response at early times, before it decays. This is shown in Figure 5 (d) below. A time-domain trace of the probe pulse described in Ref. [14] is also plotted in Figure 5 (d), demonstrating its similarity to the $\Delta\omega_c = \Delta\omega_{ps}$ case described here. From a practical perspective, it is more straightforward to make fine adjustments to the probe pulse parameters and thus achieve high spectral resolution in the *ps-ps* scheme described above than it is to control a full ultrabroad pulse, as done in the single pulse CARS method [14,15], due to the necessity of covering a broader bandwidth in the latter, and to the finite number of pixels in a spatial light modulator.

2.3 Time domain considerations

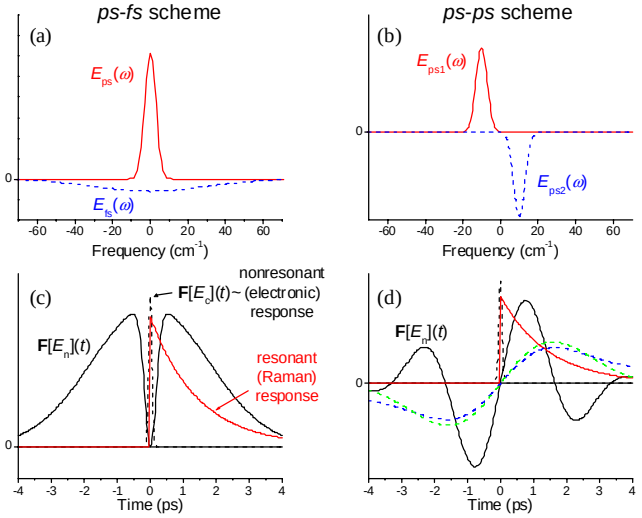

Fig. 5. (a) and (b), electric field amplitudes of probe pulses in the frequency domain for the *ps-fs* and the *ps-ps* schemes, respectively. (c) and (d), electric field amplitudes for probe and broadband pulses under NRB suppression conditions in the time domain for the *ps-fs* and the *ps-ps* schemes, respectively. The red lines in (c) and (d) represent resonant vibrational population decay, corresponding to Γ= 10 cm^{-1}. For the *ps-fs* scheme, $\Delta\omega_{ps}$ = 5 cm^{-1} and $\Delta\omega_s$ = 50 cm^{-1}. For the *ps-ps* scheme, $\Delta\omega_{ps}$ = 5 cm^{-1} and $\Delta\omega_c$ = 20 cm^{-1}. In the panel (d), the time-domain electric field amplitudes in the *ps-ps* scheme are compared between $\Delta\omega_c$ = 20 cm^{-1} (black solid line) and $\Delta\omega_c$ = 5 cm^{-1} (green dashed line). The latter is similar to the time-domain electric field amplitude of a single (frequency-domain) Gaussian probe pulse with a π phase step at the center frequency for $\Delta\omega_{ps}$ = 10 cm^{-1} (blue dashed line).

Figures 5(a) and 5(b) show time-domain electric field amplitudes for probe pulses in the *ps-fs* and *ps-ps* schemes described above. In both schemes, the probe field amplitude is zero at t=0. With probe pulses such as these, the single-shot interference CARS schemes for NRB suppression can be achieved when a well-compressed, broadband continuum pulse, $\mathbf{F}[E_c](t)$, arrives at t = 0. Under these conditions neither the 2-color resonant signal nor the NRB contributions are generated since all of these require that electric fields from all pulses (pump, Stokes, and probe) to have significant amplitude simultaneously. Survival of resonant signal in a 3-color CARS spectrum can be understood as being due to the presence of significant

#102753 - $15.00 USD Received 14 Oct 2008; revised 28 Nov 2008; accepted 4 Dec 2008; published 23 Dec 2008

probe pulse field amplitude during the non-zero lifetime the vibrational coherence set up in the sample by the continuum pulse. The Raman response function decays slowly, on the time scale of the Raman dephasing time, which typically ranges several hundreds femtoseconds to several picoseconds [21]. As Fig. 5 shows, under the NRB suppression conditions, the temporal overlap between $\mathbf{F}[E_n](t)$ and the instantaneous electronic response for NRB contribution becomes negligible compared with that between $\mathbf{F}[E_n](t)$ and the Raman response. This makes the NRB free CARS spectrum available in the 3-color broadband CARS spectroscopy.

It is clear from the time-domain description of Fig. 5 that the NRB is completely suppressed only when the continuum pulse is extremely short. A small amount of chirping is expected to increase temporal overlap between the continuum and the pulse-shaped probe pulses, resulting in residual NRB. We note that a transform-limited continuum pulse is desirable not only for removal of the NRB contribution, but significantly increases signal intensity and spectral coverage of the entire 3-color CARS spectrum [7]. However, it is difficult to generate a compressible and spectrally broad (>3000 cm^{-1}) continuum pulse from a nonlinear fiber, and these continua generally contain multiple modes with higher order dispersion [22]. The effect of non-ideal of the continuum pulse will be discussed below.

3. Experimental setup

The experimental setup is based on the previously reported two-pulse broadband CARS scheme [7,23]. Briefly, the output of a Ti:Sapphire laser oscillator (150 fs, centered at 767 nm, 76 MHz) was split into two parts. One part was introduced into a photonic crystal fiber (Femtowhite, Crystal Fibre) [24] to generate a continuum. The remaining oscillator output was dispersed into a 4*f* pulse shaper, where a reflecting spatial light modulator (CRI, SLM-640-D-NM) was used to control both amplitude and phase of probe pulses at 1.7 cm^{-1} spectral resolution and 1% amplitude resolution. The continuum and probe beams were introduced co-linearly and with parallel polarization into a 1.3 NA oil immersion objective lens. The generated CARS signal was collected using a CCD spectrometer (PhotonMax, Roper Scientific).

4. Experimental results

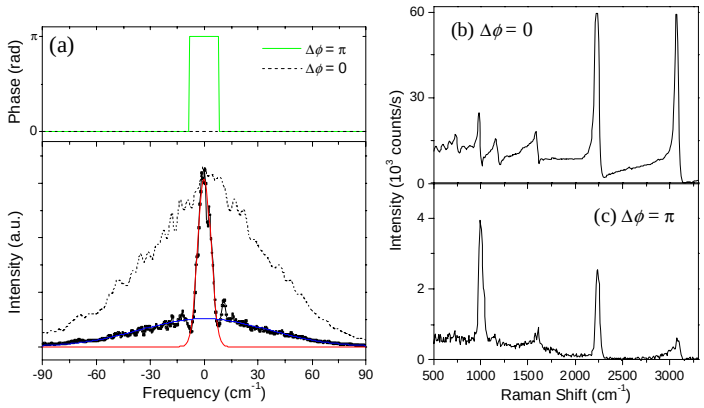

Fig. 6. (a) The original single narrowband pulse (dotted line) is decomposed into two Gaussian pulses with $\Delta\omega_{ps}$ = 10 cm^{-1} and $\Delta\omega_{fs}$ = 97 cm^{-1} for the *ps-fs* scheme (red and blue respectively). (b) and (c) - Measured broadband CARS spectra of benzonitrile at $\Delta\phi = 0$ and $\Delta\phi = \pi$ respectively. The laser power of the narrowband and the continuum pulse are 5.8 mW and 2.4 mW at the sample position. The CCD exposure time is 50 ms. Uncertainty in the wavelength calibration is ± 2 cm^{-1}.

Figure 6(a) shows the narrowband pulse for the *ps-fs* interference scheme shaped by controlling the amplitude and phase of the original femtosecond pulse (the blue dotted line)

#102753 - $15.00 USD Received 14 Oct 2008; revised 28 Nov 2008; accepted 4 Dec 2008; published 23 Dec 2008

using the spatial light modulator. The phase of the narrow center region (the *ps* component) is offset with respect to the phase of the other broad and low intensity region (the *fs* component) by a value $\Delta\phi$. Note that the pedestal *fs* component is a broad Gaussian pulse with a narrow dip at the center. Figures 6(b) and 6(c) are measured broadband CARS spectra of $\Delta\phi = 0$ and π respectively. As expected, the NRB is significantly reduced in the out-of-phase ($\Delta\phi = \pi$) CARS spectrum. Also, the resonant peaks in the NRB-suppressed CARS spectrum become symmetrical and located at the resonance frequencies as in a spontaneous Raman spectrum, so that their center frequencies do not change with experimental conditions, which could help reliable analysis of crowded Raman spectrum of complex media. We note also that peaks at higher Raman shifts are significantly reduced in the NRB suppressed spectrum. This is consistent with the simulation results of 2- and 3-color interference CARS and the characteristics of 2- and 3-color CARS signals. The higher-frequency peaks are likely to have relatively more 2-color character (see Fig. 1), and only 3-color resonant CARS signals survive at the NRB suppressing condition in the *ps-fs* interference scheme.

Figure 7(a) displays the spectrum of a narrowband pulse used to demonstrate the *ps-ps* interference scheme, where the phases of the two spectral components are independently controlled. Figures 7(b) and 7(c) show interference CARS spectra of c-hexane at $\Delta\phi = 0$ and π. These spectra also show features consistent with our simulations, such as significantly reduced NRB contribution and relatively high peak intensity at lower Raman shift, although the $\Delta\omega_{ps}$ and $\Delta\omega_c$ values were not optimized for the maximum peak intensity. The vertical lines in Fig. 7(c) indicate known spontaneous Raman resonant frequencies. We note that there appear to be many more "peaks" in the CARS spectrum in Fig. 7(b), due to spectral intensity undulations of the continuum used. Where the NRB is suppressed in Fig. 7(c), the spurious "peaks" disappear, and actual peaks become evident, slightly above the noise.

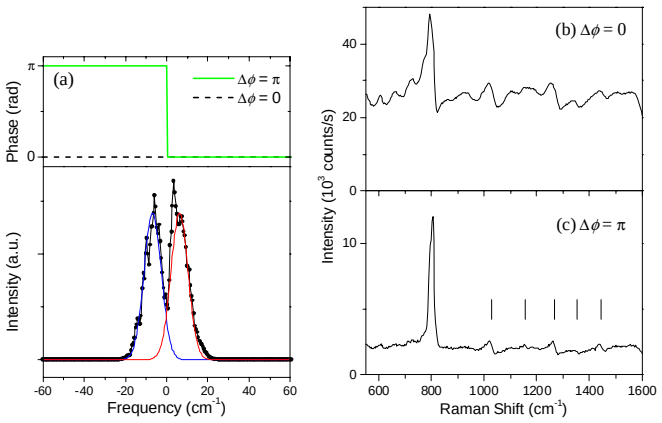

Fig. 7. (a) The measured spectrum of the narrowband pulse for the *ps-ps* scheme. Fitting the spectrum leads to two Gaussian pulses with $\Delta\omega_{ps}$ of 11 cm^{-1} and $\Delta\omega_c$ of 13 cm^{-1}. Measured broadband CARS spectra of c-hexane as a result of (b) in-phase and (c) out-of-phase interference between the two *ps* pulses. The vertical lines in the lower plot indicate spontaneous Raman resonant frequencies. The laser powers of the narrowband pulse and the continuum pulse are 7 mW and 6 mW at the sample position.

The interferometric spectra shown in Figs. 6 and 7 exhibit residual NRB. This is likely due to several factors relating to non-ideality in probe and continuum pulses. In order to satisfy the NRB compression condition for $\Delta\omega_{fs}/\Delta\omega_{ps} = 9.7$, the intended ratio of pulse intensity, I_{fs}^0 / I_{ps}^0, was 0.01 for the data in Fig. 6. While the SLM we used provides approximately 1% amplitude control, we used pulse light that was outside the antireflection coating range of the SLM, and we were able to obtain ratios only as small as 0.14. Figure 3

#102753 - $15.00 USD Received 14 Oct 2008; revised 28 Nov 2008; accepted 4 Dec 2008; published 23 Dec 2008

shows that deviations from the optimal value of I_{fs}^0 / I_{ps}^0 result in decreased resonant signal recovery and increased NRB. We experienced similar difficulties in preparing the *ps-ps* geminate pulses. Most of these problems could be avoided in an optimized experimental setup.

The more challenging issue is preparation of a transform-limited continuum pulse, which is critical, as described above. The continuum generation scheme and continuum used in this work was previously characterized by us as containing solitons [7], and was thus not entirely compressible. It is possible that this problem can be solved by new types of optical fibers [25].

5. Discussion

Control of NRB is critical for quantitative CARS microscopy, and there has been significant recent activity in both single-frequency [8] and broadband CARS applications [6]. Optimizing the signal-to-noise ratio (S/N) is typically the underlying goal when implementing NRC suppression, and, of course, both signal and noise sources should be considered [26]. The CARS signal, I_{CARS}, is proportional to the square of the sum of nonresonant and resonant susceptibility, $I_{CARS} \propto \left|\chi_{NR}^{(3)} + \chi_R^{(3)}\right|^2 = \left|\chi_{NR}^{(3)}\right|^2 + \left|\chi_R^{(3)}\right|^2 + 2\chi_{NR}^{(3)}\,\mathrm{Re}(\chi_R^{(3)})$. When the resonant signal is weak, i.e., $\left|\chi_R^{(3)}\right| << \left|\chi_{NR}^{(3)}\right|$, the CARS signal intensity is approximately proportional to $\left(\left|\chi_{NR}^{(3)}\right|^2 + 2\chi_{NR}^{(3)}\,\mathrm{Re}(\chi_R^{(3)})\right)$, and the nonresonant component serves to amplify the resonant signal intensity through the cross-term, $2\chi_{NR}^{(3)}\,\mathrm{Re}(\chi_R^{(3)})$.

For a CCD, dark noise and shot noise are the major noise sources. Dark noise is characterized as a constant background signal while shot noise is proportional to the square root of the signal intensity, i.e., $(I_{CARS})^{1/2}$. At low signal intensities, where dark noise would dominate, the noise is independent of signal intensity and a small amount of NRB may be beneficial as it could be used to amplify the resonant signal above the dark noise and improve the S/N of the measurement. On the other hand, there is little benefit in increasing signal levels through increased NRB beyond the point at which shot noise dominates because both the resonant signal and the noise increase with $(I_{NRB})^{1/2}$. Furthermore, an excessively large NRB contribution increases the ratio between the total signal, $\left(\left|\chi_{NR}^{(3)}\right|^2 + 2\chi_{NR}^{(3)}\,\mathrm{Re}(\chi_R^{(3)})\right)$, and resonant signal, $\left(2\chi_{NR}^{(3)}\,\mathrm{Re}(\chi_R^{(3)})\right)$, limiting sensitivity due to finite dynamic range of detectors and analog-to-digital converters. We note that in the large NRB contribution limit, the measured I_{CARS} is linearly proportional to a sample concentration of interest while in the NRB-free limit, I_{CARS} is quadratically proportional to a sample concentration. This can be both advantageous and disadvantageous depending on applications.

The level of NRB can be controlled in an optimized single-shot interferometric CARS apparatus by slightly detuning from the ideal NRB suppression conditions. Ultimately, the choice of how much NRB to include will be a result of balancing all experimental factors. These, with recently developed low dark-current high gain CCD detectors could make this background-free CARS technique more advantageous compared with NRB-assisted signal measurements.

The single-shot interference approach we have described can be used to obtain NRB-free spontaneous-Raman-like spectra in the fingerprint region when the 3-color CARS generation mechanism is employed. We have demonstrated this by using broadband CARS, where phase-coherence of local oscillator and signal across the broad spectral range is particularly important. The approach we describe is robust in that the signal and local oscillator are generated in the same medium, alleviating any potential issues with phase-mismatch between signal and local oscillator. Furthermore, the approach demonstrated here is not subject to the various constraints required by other methods, e.g., depolarization ratios of individual Raman modes (polarization CARS), the size and shape of the medium (epi-detection CARS), and the

#102753 - $15.00 USD Received 14 Oct 2008; revised 28 Nov 2008; accepted 4 Dec 2008; published 23 Dec 2008

Raman dephasing time (time-resolved CARS). In principle, the single-shot interference approaches can be coupled with these other CARS techniques for more specific chemical contrast.

Finally, we note that the principle of this single-shot interferometric approach can be applied to different types of pulse shaping if the integrals of electric field of the two spectral components are the same and the overall phase difference is π. An example is a single Gaussian pulse whose high frequency side has out of phase with respect to the low frequency side. These other possible schemes will have different conditions of pulse component characteristics for optimizing signal intensity and spectral resolution.

6. Conclusion

We have introduced a new interferometric approach to suppress nonresonant background in a 3-color CARS spectrum, and have demonstrated it using broadband CARS. The approach uses an amplitude-and-phase optimized pair of probe pulses, and yields background-suppressed spectra in each shot without need for phase scanning. We have demonstrated two model schemes; the *ps-fs* scheme and the *ps-ps* scheme. In both schemes, the resonant CARS signal from only the "3-color" CARS mechanism is recovered with minimal attenuation while the resonant signal from "2-color" CARS mechanism becomes negligible when the NRB contribution is suppressed. We have discussed optimization conditions for the signal intensity and shape of resonant peaks. Experimental CARS spectra of c-hexane and benzonitrile obtained by preliminary measurements are consistent with the simulation results, showing NRB-suppressed CARS spectra.

Acknowledgment

We thank NIH (R21 EB002468-01) for financial support.

#102753 - $15.00 USD Received 14 Oct 2008; revised 28 Nov 2008; accepted 4 Dec 2008; published 23 Dec 2008